

MICRO-TENSILE TESTING OF NANOCRYSTALLINE Al/Zr ALLOYS

M. Legros*, K. J. Hemker*, D. A. LaVan*, W. N. Sharpe, Jr.*, M. N. Rittner**, and J. R. Weertman**;

*Dept. of Mechanical Eng., Johns Hopkins University, Baltimore, MD 21218-2686,

**Dept. Of Materials Science and Eng., Northwestern University, Evanston, IL 60208-3108.

ABSTRACT

A novel micro testing machine has been used to perform tensile tests on nanocrystalline Al/Zr microsamples with grain sizes ranging from 10 to 250 nm. The problems associated with testing such small specimens (200 μ m x 200 μ m in the gage section) were overcome by using a contact-free interferometric strain gage (ISDG) and alignment and low friction loading were assured by use of a linear air bearing. The postulated relationship between yield stress and hardness was investigated and will be discussed. The effect of the microstructure and the grain size of the compacts on their mechanical behaviour are also analysed.

INTRODUCTION

By reducing the free path of dislocation motion in a crystalline material, one can expect to increase its resistance to deformation and therefore enhance its mechanical properties such as hardness and yield strength [1,2]. Grain boundaries offer formidable obstacles to dislocation motion and the effect of grain sizes in mechanical strength is generally described by the Hall-Petch (HP) relationship [3-7], which has been evidenced in many materials and especially metals [8-12]. The hardness of nanocrystalline metals has been widely investigated this past ten years and it has been suggested that hardness follows the HP relationship down to a critical grain size [4]. When a grain size of several nanometers is reached, the hardness of the nanocrystalline material, as compared to the coarse grain material, can be magnified by a factor as high as 6 to 10 [4]. A parallel increase in yield stress has been projected from these unusually high hardness values. Unfortunately, nanocrystalline metals are generally produced in very small quantities and for this reason very few compressive tests and even fewer tensile tests have been performed to date [9,13-17].

The recent development of a novel microsample testing machine has greatly facilitated the mechanical testing of very small specimens [18]. Dog-bone tensile specimens with a gage section of approximately 250 μ m x 250 μ m and an effective gage length of 1.8 mm can be pulled in tension using a load frame that applies loads on the order of 20 pounds and measures strain using a non-contact interferometric strain gage (ISDG). This test set-up assures proper alignment and low friction loading of the specimen by use of a linear air bearing. The ISDG strain measurement device is a critical component of this testing because it provides a means in which displacement can be measured directly on the sample surface without actually touching the sample and interfering with the testing. The resolution of this system is approximately 0.5 MPa and 10 μ strain, which make it an ideal technique for surpassing the geometrical hurdles associated with the tensile testing of very small nanocrystalline samples.

The purpose of this study was to take nanocrystalline Al and Al-Zr specimens that have been prepared at Argonne National Laboratory using inert gas condensation (IGC) and uniaxial compression and to perform microsample tensile tests on these materials. This project has been further expanded to include a comparison of the results of these tensile tests with microhardness measurements and TEM microstructural observations of the same nanocrystalline materials. Here, emphasis will be placed on stress-strain curves obtained on compacts with grain sizes ranging from 10 to 250 nm, and a comparison of these results with tensile tests made previously from somewhat larger pieces of the same material at Northwestern University [17].

EXPERIMENTAL

Material processing

The alloys tested in this study were prepared at Northwestern University. Precursor powders of Al and Zr were produced using the Inert Gas Condensation (IGC) technique [11, 16]. After evaporation by electron-beam heating and condensation on a liquid nitrogen cold finger, the nanocrystalline mixed metals were scraped off of the cold finger and collected in powder form. These powders were transported, under high vacuum, to a heatable die that was employed for compaction. The powders were uniaxially pressed under 1.4 GPa at 100 °C [16]. The resulting disks were 9mm in diameter and 100 to 800 μm thick. Their average relative density was determined to be always greater than 93%.

Since pure nanocrystalline Al was found to exhibit grain growth, even at room temperature, small amounts of Zr were added to the Al in an attempt to stabilize the grain size of the alloys and keep it in the nanometer regime [16]. The Zr was added during evaporation by periodically moving the electron beam from the Al to the Zr crucible. Chemical analysis and grain size determination of the Al-Zr alloys were performed using both x-ray diffraction [16] and electron microscopy (TEM). The average oxygen and Zr contents are reported along with the corresponding grain sizes in Table 1. Oxygen was found to be mainly located at the free surface of the pellet, especially in cases where the average O content was beyond 4 -5 wt.%. Room temperature stability of the as-produced Al-Zr samples was verified by comparing the TEM microstructure taken a few weeks after processing with that conducted more than one year after fabrication. There was no visible change in the microstructure. Moreover, *in-situ* TEM heating experiments revealed that no significant grain growth takes place at temperatures below 400°C [16] in the case of samples containing several % or more of Zr.

Preparation of microsample tensile specimens

The as pressed pellets were initially sectioned to produce a small but conventional tensile specimens (4mm x 7mm) that were tested using a conventional MTS machine at Northwestern University. The results of these tests, which were conducted with small strain gages glued to the flat face of the gauge section, have been published elsewhere [16, 17]. Dog-bone shaped microsample tensile specimens (Fig. 1) have been punched out of the left-over wings of the nanocrystalline pellets. The punching of these delicate specimens is greatly facilitated by the use of a specially machined graphite electrode on a plunger EDM that is equipped with a Micro Fin power controller. The punched specimens are mechanically polished to a mirror finish and a final thickness of ~ 200 μm. Once polished, two small reflective markers, microhardness indents, are placed on the nanocrystalline specimens using a Vickers microhardness indenter. These indents serve as reflective markers for the interferometric strain displacement gage (ISDG) [20].



Fig. 1 : SEM picture of a micro tensile specimen. The gauge section is 200 x 200 μm.

The microsample tensile machine

The microsample testing machine provides a method in which micro scale samples can be tested in both tension and compression [21, 24]. The testing machine consist of the basic components found in a typical testing frame, but have been scaled down to handle the unique demands associated with micron scale testing. The microsample load frame is actuated by a low speed screw drive and employs an air bearing that maintains alignment and reduces friction so that

loads on the order of .001 lb can be measured. The load is measured directly with a miniature load cell. The dog-bone shape of the specimens allows the ends of the specimen to fit into matching wedge-shaped grips and the specimen seats itself into the grip when pulled in tension. The complete description of this machine can be found in [19-21].

Table 1: Average chemical composition, density and grain size of the nanocrystalline alloys used in this study.

Sample	Zr wt. %	O wt. %	% Density	GS (nm)
A	0	2	98	250
B	7	2	97	10
C	7	2	97	70
D	15	2	95	20
E	31	1	94	15

The principle of the ISDG consists of measuring the relative displacement of two reflective features, microhardness indents, on the specimen. Shining a laser on the specimen leads to diffraction of the coherent beam and results in a fringe pattern. The relative displacement of these fringes can be measured using a photodiode array and related to the strain in the specimen. The relative displacement of the fringes (Δm) is related to the strain of the specimen (ϵ)

$$\text{by the relation : } \epsilon = \lambda \Delta m / d_0 \sin \alpha_0 \quad (1)$$

where α_0 is the angle between the incident beam and the indent facets, d_0 is the initial spacing between indents and λ the wavelength of the laser [20, 21]. By averaging the relative displacement on two diode arrays, resolution on the order of microstrain can be achieved. Specimen bending can be accounted for by measuring the strain on both sides of the sample [22].

Microstructural characterization

Electron microscopy (TEM and EDX) and x-ray diffraction (XRD) have been used to analyse the chemical composition and underlying micro(nano)structure of the specimens tested in this study. TEM samples have been prepared by either electropolishing or use of a tripod polisher and subsequent ion-milling.

RESULTS AND DISCUSSION

The chemical composition and average grain size of the different samples tested are reported in Table 1. These values were obtained by using EDS on the as-pressed samples, and are reported in greater detail in [16].

Systematic arrays of microhardness indents were used to measure variations in hardness for each of the nanocrystalline alloys. Hardness values for all alloys are reported in Table 2. A dual distribution of hardness values was evidenced in the higher Zr containing alloys. This variation in hardness was not random; instead the overall specimens could be divided into harder and softer regions. Fig. 2 is the plot of hardness expressed in GPa as a function of $d^{-1/2}$, where d is the average grain size. As can be seen, the average values of hardness for the different alloys seems to follow a Hall-Petch relationship down to sample D. However, the measured values of hardness were found to have a bi-modal distribution at smaller grain sizes, and the evidence of a HP behavior appears to be much less conclusive than is suggested by the averaged data.

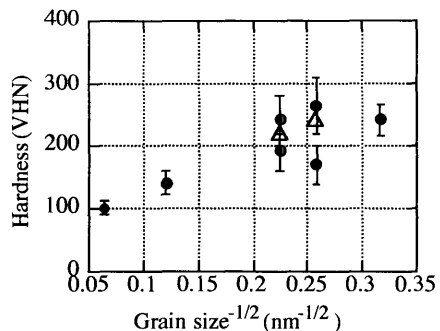


Fig. 2 : Hardness as a function of $d^{-1/2}$ for samples A-E. Triangles represent average values of H for spec. D, E.

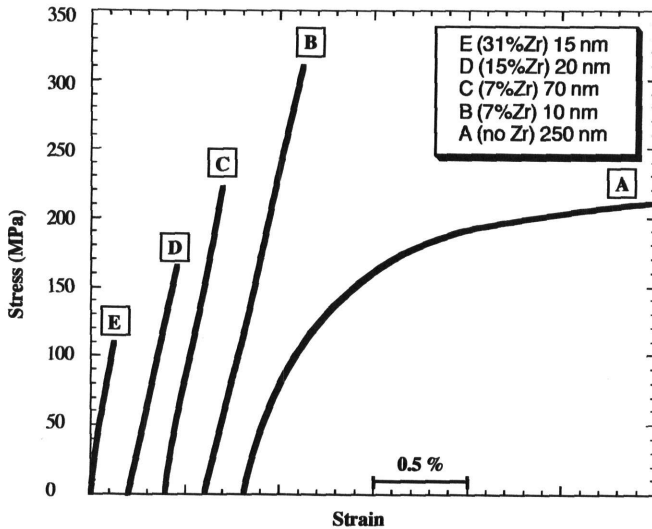


Fig. 3 : Tensile stress-strain curves of nanocrystalline alloys A-E.

[27]. By contrast, the stresses realized in these tests are significantly higher than the generally referenced value of the yield strength of bulk aluminum ($\sigma_y=20$ MPa). The stress-strain curve for nanocrystalline aluminium (A) exhibits nonlinear permanent deformation and is suggestive of dislocation motion and plasticity. By comparison, the Al-Zr alloys remained very linear and fractured with very little or no plasticity. This lack of plasticity, even at very high stresses, had been taken as a strong indication that dislocation motion is effectively inhibited or blocked in these nanocrystalline alloys. This brittle behaviour is expected when the size of the grains of a previously ductile metal is reduced to the nanometer scale [4, 23]. It is however, interesting to note that the fracture strength decreases with increasing Zr content, as seen on Fig. 5, which emphasizes the role of the flaws in this type of alloy [28]. Material from the same disks as used for samples A and B had been tested previously at Northwestern. The slightly higher values reported here, especially in the case of the more ductile sample (A) have been attributed to a miscalibration of the compliance of the glue and the strain gauge used in the previous study (but the maximum strains have been found to be very close). The fracture stresses of sample B are in decent agreement between the two studies (250 Mpa compared to 300 Mpa here).

A semi-empirical relation between hardness and yield stress has been established for non hardening materials in the case of a pyramidal indenter [26]. This relation states that the yield stress σ_y can be obtained from hardness (H) by converting from VHN to GPa and dividing by a factor generally close to 3 [26]. Although this relationship between H and σ_y has been found to hold in compression tests of some nanocrystalline metals [13], it has not been validated in the small

Table 2 : Mechanical properties collected from tensile tests and Vickers indentations.

Sample (Grain size)	A (250 nm)	B (10 nm)	C (70 nm)	D (20 nm)	E (15 nm)
Hardness (converted from VHN to GPa)	1.04 ±.12	2.40 ±.20	1.25 ±.20	2.50 ±.15*	2.60 ±.20*
Young's modulus (GPa)	68 ±5	69 ±3	72 ±5	69 ±4	71 ±6
Max strain (%)	2.4	0.6	0.3	0.25	0.13
Yield Stress(MPa)	75				
Fracture stress (MPa)	200	315	220	165	110

* The average values of hardness for samples D and E are respectively 2.20 GPa (±.60) and 2.40 GPa (±.60)

number of tensile tests that are available in the literature [14-16]. In the present study, the ratio of hardness (1 GPa) and tensile yield strength (75 M Pa) for the nanocrystalline Al alloy (A) has been measured to be 13. The fact that this ratio is not 3 suggests that this empirical relationship may not be appropriate for all nanocrystalline materials and may be explained, at least in part, by the fact that alloy A can be seen to undergo significant strain hardening on the stress-strain curve in Fig. 3. The fact that alloys B-E fractured before yielding precluded comparing them with their hardness values, and served to highlight the importance of fracture in nanocrystalline materials.

Microstructural observations

TEM observations have been used to characterize the underlying micro(nano)structure of the alloys tested in this study. Fig. 4 is a TEM micrograph of alloy B. This alloy appeared to be the most homogeneous of the Al-Zr alloys when observed with an optical microscope and SEM, but TEM observations like the one shown in this figure indicate significant variations in the microstructure. Three different regions (marked I, II and III) can be seen in this micrograph, and grain sizes in these regions range from about 5nm (I) to more than 100nm (III). This variation in grain size has been directly related to the local concentration of Zr; the the larger the concentration of Zr the smaller the grain size. In addition, two oxides Al_2O_3 and ZrO_2 and one intermetallic Al_3Zr were found to coexist with the main Al phase. But, by using dark field imaging the volume fraction of these phases compared to Al was only estimated to be on the order of a few percent. The size and shape of the grains of these second and third phases were generally found to scale the grain size of the Al phase. These observation are consistent with those reported previously on the same material.

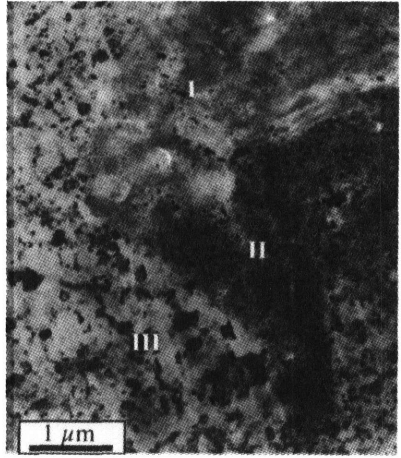


Fig. 4 : Multi modal nanostructure of sample B. The number I, II and III are related to zones of different average grain sizes.

The relationships between the underlying micro(nano)structure and the various mechanical properties that have been measured in this study can be reasoned as follows. The bimodal distribution of hardness that has been measured in alloys D and E (and to a lesser extent C) may be caused by the spacial distribution of grain sizes; areas with smaller grain sizes are harder while those with bigger grain sizes are softer. This is supported by the fact that areas with the similar hardness values generally coincided with areas that exhibited a constant optical contrast, while changes in optical contrast (relating to changes in local average grain size) generally related to changes in hardness. By contrast, changes and variations in grain size did not have an effect on the elastic modulus that was measured in the microsample tensile tests. Although small, the cross-section of the microsample specimens contained more than one million grains and small changes in the size and distribution of these grains would not be expected to affect the measurement of Young's modulus. The effect of microstructure on fracture strength can perhaps best be divided into two parts. Increasing the Zr content in the alloys not

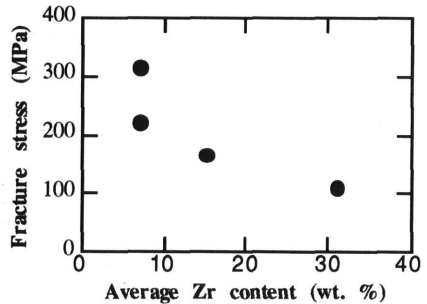


Fig. 5 : Fracture stress as a function of Zr content for samples B-E.

only decreased the grain size but also increased the heterogeneity of the material. Of the two, the effect of having a heterogeneous microstructure appears to be more influential. As can be seen in Fig. 5, the material fails faster at higher levels of Zr concentration.

CONCLUSIONS

1. The addition of Zr to nanocrystalline Al reduced grain growth but also led to a more heterogeneous micro(nano)structure.
2. Young's modulus of the alloys tested in this study were not affected by variations in the grain size or the heterogeneity of the micro(nano)structure.
3. Like microhardness, the yield strength of nanocrystalline Al is significantly higher than for bulk Al. But the empirical yield strength to hardness ratio of 1/3 was not observed in this alloy. The measured ratio in this study was close to 1/14.
4. Yielding was suppressed in the nanocrystalline Al-Zr alloys and fracture appeared to be related to inhomogeneities in the microstructure more than to the average grain size.

REFERENCES

1. J. R. Weertman, *Mat. Sci. and Eng.*, **A166**, 161-167, (1993)
2. R. W. Armstrong, *Mat. Res. Soc. Symp. Proc.*, **362**, 9-17, (1995)
3. J. C. M. Li, Y. T. Chou, *Metall. Trans.*, **1**, 1145-1158, (1970)
4. R. W. Siegel, G. E. Fougere, *Mat. Res. Soc. Symp. Proc.*, **362**, 219-229, (1995)
5. T. R. Smith, R. W. Armstrong, P. M. Hazzledine, R. A. Masumura, C. S. Pande, *Mat. Res. Soc. Symp. Proc.*, **362**, 31-37, (1995)
6. A. H. Cholski, A. Rosen, J. Karch, H. Gleiter, *Scripta Met.*, **23**, 1679 (1989)
7. J. Lian, B. Baudalet, *Nanostructured Materials*, **2**, 415-419, (1993)
8. G. E. Fougere, J. R. Weertman, R. W. Siegel, *Nanostructured Materials*, **5**, 2, 127 (1995)
9. A. Kumpmann, B. Günther, H. D. Kunze, in *Mechanical Properties and Deformation Behavior of Materials Having Ultra-Fine Microstructures*, M. Nastasi et al. eds, 241-254, Kluwer Academic Publishers, (1993)
10. L. Wong, D. Ostrander, U. Erb, G. Palumbo K. T., Aust, in *Nanophases and Nanocrystalline Structures*, R. D. Schull and J. M. Sanchez eds, 85-93, The Minerals, Metals & Materials Society, (1994)
11. B. Günther, A. Baalman, H. Weiss, *Mat. Res. Soc. Symp. Proc.*, **195**, 611, (1990)
12. C. Suryanarayana, F. H. Froes, *Metall. Trans.*, **23A**, 1071-1081, (1992)
13. R. Suryanarayanan, Ph. D. thesis, Washington University at St Louis (1996)
14. G. W. Nieman, J. R. Weertman, R. W. Siegel, *Scripta Metall.* **23**, 2013 (1989)
15. G. W. Nieman, J. R. Weertman, R. W. Siegel, *J. Mater. Res.* **6**, 1012 (1991)
16. M. N. Rittner, Ph. D. thesis, Northwestern University (1996)
17. M. N. Rittner, J. R. Weertman, J. A. Eastman, K. B. Yoder, D. S. Stone, to appear in *Mat. Sci. and Eng.*
18. W. N. Sharpe, R.O. Fowler, ASTM STP 1204, *Small Specimen Test Techniques Applied to Nuclear Reactor Vessel Thermal Annealing and Plant Life Extension*, (1993), 386-401.
19. C. C. Koch, T. D. Shen, T. Malow, O Spaldon, *Mat. Res. Soc. Symp. Proc.*, **362**, 253-264, (1995)
20. Sharpe, W.N., Jr., *NASA Technical Memorandum*, 101638, (1989).
21. Sharpe, W.N., Jr., B. Yuan; Accepted in *Nontraditional Methods Of Sensing Stress, Strain and Damage in Materials and Structures*, SATM STP 1318, G. F. Lucas and D. A. Stubbs, Eds., ASTM Philadelphia 1997
22. D. A. LaVan, W. N. Sharpe, to appear in *SEM proceedings ...*(1997)
23. M. A. Otooni, *Mat. Res. Soc. Symp. Proc.*, **362**, 45-49, (1995)
24. M. Zupan, K. J. Hemker, *Mat. Res. Soc. Symp. Proc.*, symposium Z, this conf., (1996)
25. M. N. Rittner, J. R. Weertman, J. A. Eastman, *Acta Mater.*, **44**, n° 4, 1271-1286, (1996)
26. F. A. Mc Clintock, A. S. Argon, *Mechanical behaviour of materials*, Addison-Wesley Pub. (1966)
27. C. J. Smithells, *Metals reference book*, Butterworths, London, (1976)
28. J. R. Weertman, M. N. Rittner M. and C. Youngdahl, in *Mechanical Properties and Deformation Behavior of Materials Having Ultra-Fine Microstructures*, M. Nastasi et al. eds, 241-254, Kluwer Academic Publishers, (1993)